Matter

CellPress

Article

Spontaneous Non-stoichiometry and Ordering in Degenerate but Gapped Transparent Conductors

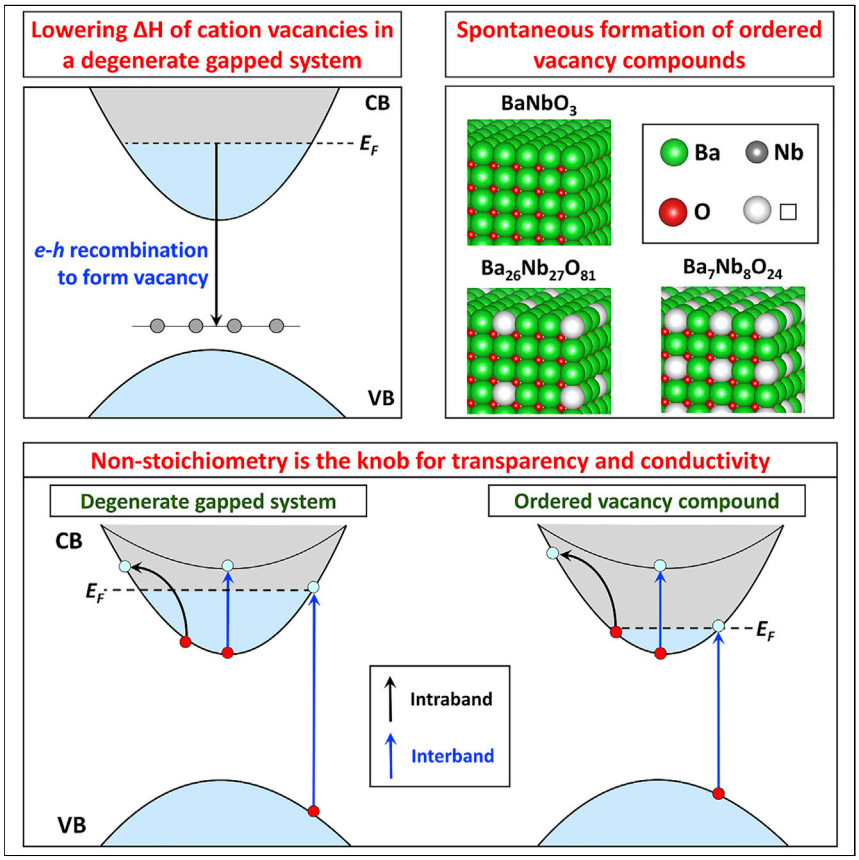

Formation of non-stoichiometric compounds is often thought to be a growth effect rather than a specific electronic instability. We demonstrate that degenerate gapped compounds with large internal gap and Fermi level in the conduction band can have spontaneous non-stoichiometry, even at low temperatures, due to decay of a fraction of the free electrons into the hole states formed by such vacancies. This unique material feature allows controllable non-stoichiometry to be used to archive target material stability and optoelectronic properties for transparent conductors and electrides.

Discovery
A new material or phenomena

Oleksandr I. Malyi, Michael T. Yeung, Kenneth R. Poeppelmeier, Clas Persson, Alex Zunger

oleksandrmalyi@gmail.com (O.I.M.)
alex.zunger@colorado.edu (A.Z.)

HIGHLIGHTS

Carriers in degenerate gapped compounds can cause spontaneous non-stoichiometry

Spontaneous non-stoichiometry can result in formation of ordered vacancy compounds

Different ordered vacancy compounds can be realized by controlling growth conditions

Controllable non-stoichiometry is the knob that tunes transparency and conductivity

Malyi et al., Matter *1*, 280–294
July 10, 2019
https://doi.org/10.1016/j.matt.2019.05.014

Matter

CellPress

Article

Spontaneous Non-stoichiometry and Ordering in Degenerate but Gapped Transparent Conductors

Oleksandr I. Malyi,[1,2,*] Michael T. Yeung,[3] Kenneth R. Poeppelmeier,[3] Clas Persson,[2] and Alex Zunger[1,4,*]

SUMMARY

We highlight a class of materials representing an exception to the Daltonian view that compounds maintain integer stoichiometry at low temperatures and use this behavior to select ordered vacancy compounds (OVCs) striking a wanted compromise between carrier concentration, transparency, and phase stability, crucial for transparent conductors (TCs). We show that carriers in the conduction band (CB) of degenerate gapped $BaNbO_3$, $Ca_6Al_7O_{16}$, and $Ag_3Al_{22}O_{34}$ compounds can cause a self-regulating instability, whereby cation vacancies form exothermically because a fraction of the CB electrons decays into the hole states formed by such vacancies, and this electron-hole recombination offsets the positive energy associated with vacancy bond breaking. This Fermi level-induced spontaneous non-stoichiometry can lead to the formation of OVCs with different optoelectronic properties and stable in different ranges of chemical potentials. Thus, we demonstrate how a window of opportunity can be determined between opposing tendencies of transparency, conductivity, and stability to design TCs.

INTRODUCTION

Spontaneous Non-stoichiometry as a Fermi Level Instability

The fact that compounds manifest integer ratios between component elements (the law of definite proportions[1]) has been the cornerstone of our understanding of formal oxidation states (taking up integer values) and defect physics (showing that violation of integer ratios by formation of defects costs energy and is thus unlikely at low temperatures). This thinking of the Daltonides school (the paradigm of stoichiometry) stood in stark contrast with the non-stoichiometric Berthollides[2] school, who argued that compounds could possess a range of compositions entirely dependent on the starting synthetic conditions. We point out an interesting class of exceptions to the Daltonide universal understanding, whereby a degenerate but gapped compound with Fermi energy (E_F) inside the conduction band (CB) and a large internal band gap (E_g^{int}) between the valence band maximum (VBM) and conduction band minimum (CBM) (as shown in Figure 1A) could form a significant concentration of low-energy vacancies, violating the rule of integer stoichiometry.

This understanding has an important implication on transparent conductors (TCs),[3] those rare compounds in which the generally mutually exclusive properties of optical transparency (usually common only in electrical insulators) and conductivity (usually common only in opaque metals) coexist. This internal contradiction has been the reason why finding good TCs has proven to be so difficult. The old class of TCs was developed by starting with an insulator (such as In_2O_3 or ZnO, schematically shown

Progress and Potential

Degenerate gapped compounds, those with their Fermi levels inside the conduction band and sufficiently large "internal band gaps" below this Fermi level, are shown here to have negative formation enthalpy for cation vacancies, leading to spontaneous non-stoichiometry and formation of characteristic ordered vacancy compounds (OVCs), even at low temperature, in defiance of Daltonian stoichiometry. Selection during the growth of a specific OVC can be used to mitigate the notoriously difficult conflict between transparency and conductivity, with potential interests beyond of transparent conductors, including electrides and photocatalysts. This surprising prediction is validated with two key experimental findings: silver beta-alumina $Ag_3Al_{22}O_{34.5}$ leeches out silver atoms upon any attempt to introduce electron carriers, whereas a number of different OVC structures stabilized by effective reconstructions are observed during the synthesis of the tetragonal tungsten bronze $Ba_3Nb_5O_{15}$.

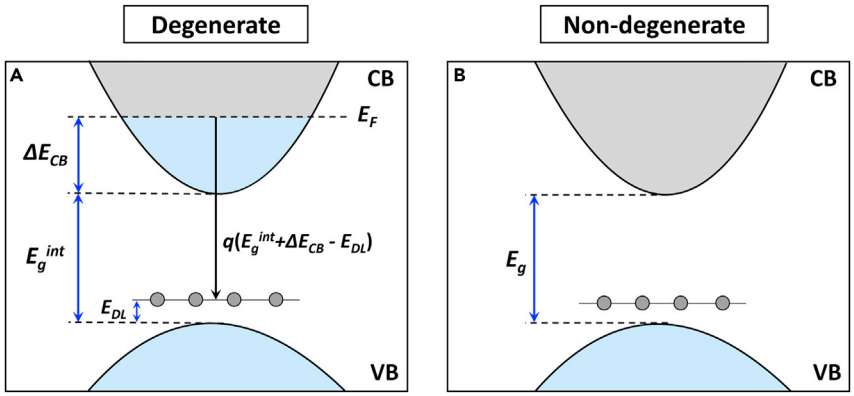

Figure 1. Mechanism for Lowering Formation Energy of an Acceptor in Degenerate Gapped Material
Schematic illustration of defect formation in (A) degenerate gapped compounds and (B) non-degenerate gapped insulators, showing lowering defect formation energy governed by removing an electron from the conduction band. Blue (gray) areas represent occupied (empty) states. Here, ΔE_{CB} is the occupied part of the conduction band; E_g^{int} is the internal band gap, and E_{DL} is the electron-trap defect level produced by, e.g., cation vacancies.

in Figure 1B) and then attempting heavy doping (by Sn or Al, respectively), making it conductive. This has faced severe "doping bottlenecks,"[4] whereby intended doping by electrons creates "electron killers" in the form of intrinsic acceptors. An alternative strategy[5] is to start from a metal (Figure 1A) and attempt to make it transparent, avoiding doping bottlenecks. The deeper understanding of spontaneous non-stoichiometry discussed here clarifies that the latter approach can present an unusual window of opportunity, whereby (1) transparency, (2) conductivity, and (3) phase stability can coexist and be selected by zooming in on specific growth conditions (chemical potentials). Specifically, a compound that has the Fermi level inside the CB (a nominal band conductor with free electrons) could become opaque because too many electrons create a strong plasma absorption in the visible range. But if this compound also has a sufficiently large internal band gap below the Fermi energy (i.e., being degenerate but gapped, Figure 1A), it will create spontaneous defects (here, cation vacancies that are hole-producing acceptors) that, while violating Daltonian stoichiometry, also regulate the carrier concentration by compensating the native electrons via the spontaneously produced holes. It is the exothermic electron-hole compensation reaction that drives non-stoichiometry. Unlike the case of the limited formation of dilute vacancies in ordinary insulators (Figure 1B), if there is an internal gap (Figure 1A), then, at the concentrated limit, such vacancies can condense into ordered crystallographic arrays (Figures 2A and 2B), thus explaining the hitherto peculiar occurrence[6] of macroscopically observed sequences of ground state ordered vacancy compounds (OVCs),[7–10] such as $Ba_lNb_mO_n$, with l:m:n ratios of 1:2:6, 3:5:15, 5:4:15, 7:6:21, 7:8:24, 9:10:30, and 26:27:81. We highlight cases in which the vacancy ordering is clearly visible (Figure 2B) versus cases in which, following vacancy ordering, further total energy relaxation yielded structural changes (reconstruction) that make it difficult to visualize the original vacancy ordering. These otherwise peculiar integer ratios emerge as stable, T = 0 K ground state structures obtained via a first-principles total energy search. It turns out that such cation vacancy compounds occur as a sequence of discrete phases, each with its own vacancy concentration (e.g., 7:8:24, 9:10:30, and 26:27:81, with 12.5%, 10%, and 3.7% of Ba vacancies, respectively) and each is stabilized at specific reactant chemical potentials (colored domains in Figure 2A). Because of the discrete vacancy ratios, each phase, as illustrated below, has its characteristic residual (post-compensation) electron

[1]Renewable and Sustainable Energy Institute, University of Colorado, Boulder, CO 80309, USA

[2]Centre for Materials Science and Nanotechnology, Department of Physics, University of Oslo, PO Box 1048 Blindern, 0316 Oslo, Norway

[3]Department of Chemistry, Northwestern University, Evanston, IL 60208, USA

[4]Lead Contact

*Correspondence: oleksandrmalyi@gmail.com (O.I.M.), alex.zunger@colorado.edu (A.Z.)

https://doi.org/10.1016/j.matt.2019.05.014

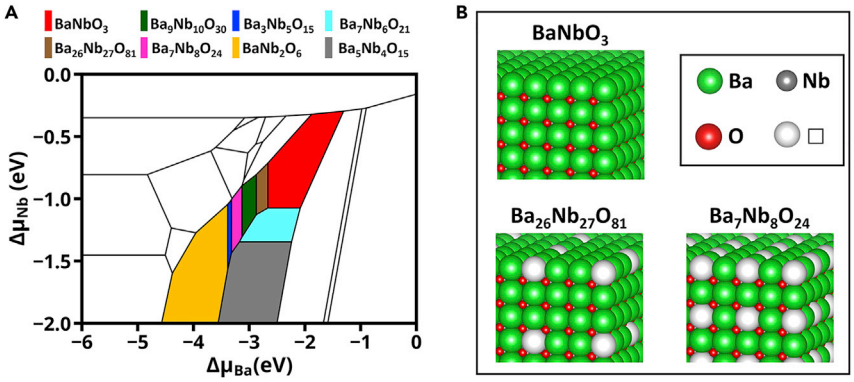

Figure 2. Formation of Stable OVCs in the Ba-Nb-O System

(A) Chemical potential diagram for the Ba-Nb-O system, showing stability chemical potential zones for $BaNbO_3$ and each stable OVC phase.

(B) Crystal structures of $BaNbO_3$ and its unreconstructed OVCs demonstrating long-range ordering of Ba vacancies.

concentration and optical response. Such phases (Figure 2A) could then, in principle, be selected during growth by targeting the requisite cation chemical potential, so that the desired optoelectronic properties can be achieved. This work demonstrates that controlled deviation from Daltonian stoichiometry can be used as a knob to regulate transparent conductivity. We validate our theory with two key experimental findings: silver β-alumina $Ag_3Al_{22}O_{34.5}$ leeches out silver atoms forming Ag vacancies upon any attempt to introduce electron carriers, and tetragonal tungsten bronze $Ba_3Nb_5O_{15}$, in which the cation vacancy formation favors the formation of secondary phases. Our paper is the first attempt to understand and unravel the intrinsic complex connection between stoichiometry and properties, creating a roadmap for the future. This work has broad implications, as degenerate gapped compounds have been generating increasing interest in many fields beyond that of TCs, including the colored metallic photocatalysts as seen in the substoichiometric $Sr_{1-x}NbO_3$,[11] the electron-donating promotors for catalysts[12] to low work function compliance layers.[13] Furthermore, our work explains why many of these degenerate gapped compounds require exotic synthesis conditions to be prepared stoichiometrically.

RESULTS AND DISCUSSION

Dilute Metal Vacancies Can Form Readily in Degenerate Gapped Compounds

The formation of vacancies in ordinary insulators (Figure 1B) involves breaking of stable chemical bonds without restoring any of the spent energy, so a significant concentration of such defects can exist only at increased temperatures. The situation can be different in degenerate gapped compounds (with E_F located at an energy ΔE_{CB} above the CBM, as in $BaNbO_3$, $Ca_6Al_7O_{16}$, and $Ag_3Al_{22}O_{34}$ discussed below) with an internal band gap E_g^{int} between the CBM and VBM (Figure 1A). Here, the formation of dilute concentration of metal vacancies can create electron acceptor states near the valence band (at energy E_{DL}), resulting in the opportunity for decay of q CB electrons into these electron acceptor states, thereby regaining the energy $q(E_g^{int} + \Delta E_{CB} - E_{DL})$, which reduces the vacancy formation energy accordingly (see Figure 1A). When this energy exceeds the bond-breaking energy, one expects spontaneous non-stoichiometry. This defines an electronic Fermi level mechanism for Berthollides[2] non-stoichiometry.

To validate this concept, Figures 3A, 3C, and 3E show the results of density functional calculated formation energies of the Ba vacancy in $BaNbO_3$, the Ca vacancy

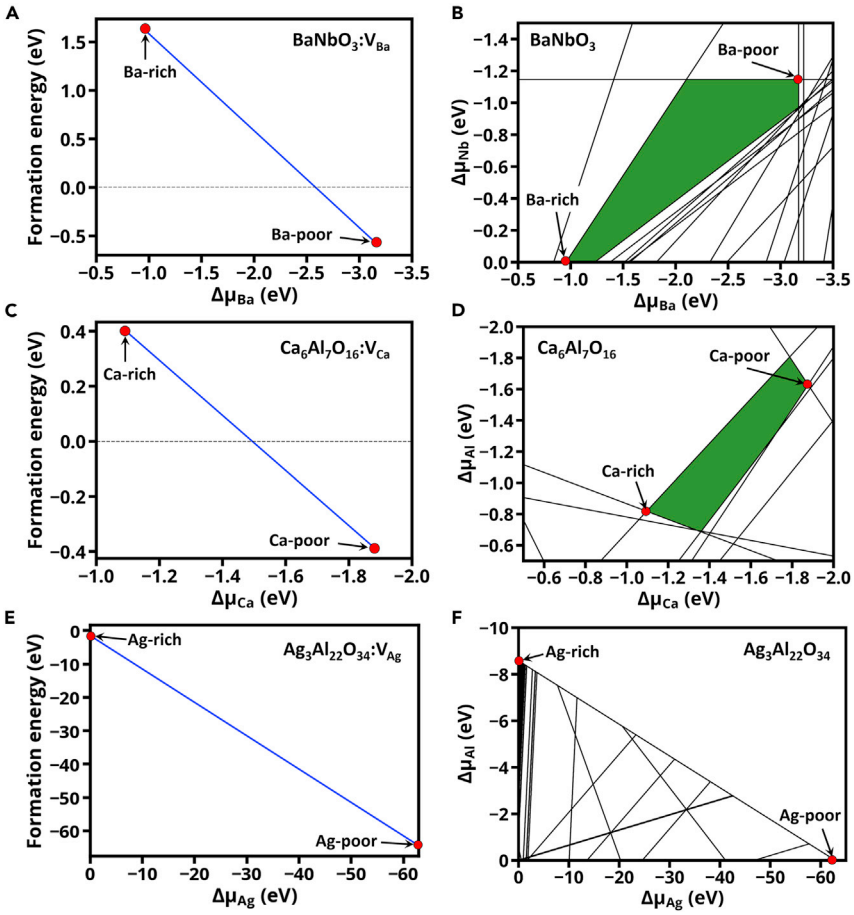

Figure 3. Spontaneous Vacancy Formation in Degenerate Gapped Insulators

Metal vacancy formation energy (left-hand panels) and region of chemical potentials (green zone) where the degenerate gapped insulator is stable (right-hand panels) for (A and B) $BaNbO_3$, (C and D) $Ca_6Al_7O_{16}$, and (E and F) $Ag_3Al_{22}O_{34}$. For $Ag_3Al_{22}O_{34}$, no green zone exists where the compound is stable. Only experimentally observed stoichiometric phases are used to calculate the ranges of chemical potentials under which the compounds are stable.

in $Ca_6Al_7O_{16}$, and the Ag vacancy in $Ag_3Al_{22}O_{34}$, as a function of the metal chemical potential (see Experimental Procedures). The allowed stable chemical potential regions (constructed by considering possible competing phases, see Experimental Procedures) of the respective bulk compounds are shown in Figures 3B, 3D, and 3F. We see that for the degenerate gapped compounds under cation-deficient chemical potential conditions, vacancy formation energies can be extremely low (in fact, negative). Whereas $BaNbO_3$ and $Ca_6Al_7O_{16}$ have stable chemical potential (green) zones at the respective stoichiometries indicated, $Ag_3Al_{22}O_{34}$ does not. In fact, in the latter case, the Ag vacancy formation energy (Figure 3E) is so strongly negative under all chemical potential conditions, that the CB is empty and the parent degenerate $Ag_3Al_{22}O_{34}$ phase is not stable (i.e., no green zone in Figure 3F).

Dilute Vacancies Can Condense into Stable OVCs Forming Homological Sequences

The negative formation energies of dilute vacancies open the possibility of vacancy condensation and long-range ordering (Figure 2B). To examine this possibility, we have calculated the T = 0 K stable phases ("ground state diagram" or "convex

Composition	Synthesis	Characterization	Possible OVC	RT Properties
Ba-Nb-O				
$BaNbO_3$[15,16]	Evacuated quartz tube, 1117 °C	pXRD	No	-
$Ba_{0.95}NbO_3$[17]	Flux growth, vacuum furnace	SC-XRD	Yes	-
$Ba_{0.97}NbO_3$[18]	Evacuated quartz tube, 1200 °C	pXRD	Yes	Metallic
$Ba_3Nb_5O_{15}$[19]	Flux growth, vacuum furnace	SC-XRD	Reconstructed	Semiconductor
$Ba_6Nb_{10}O_{30}$[20]	Evacuated quartz tube, 1100 °C	pXRD	Reconstructed	Semiconductor
$Ba_6Nb_{10}O_{30}$[21]	Evacuated quartz tube, 1200 °C	EDS, pXRD	Reconstructed	Semiconductor
$Ba_6Nb_{10}O_{30}$[22,23]	Low P_{O_2} sintering, 1360 °C	pXRD	Reconstructed	Metallic
$Ba_6Nb_{10}O_{30}$[24,25]	Low P_{O_2} sintering, 1300 °C	pXRD, TEM, EDS	Reconstructed	Semiconductor
$BaNb_2O_6$[26]	Flux growth, 1450 °C	SC-XRD	Reconstructed	Semiconductor
$Ba_5Nb_4O_{15}$[27]	Sintering, 1150 °C	pXRD	Reconstructed	Semiconductor
Ca-Al-O				
$Ca_{12}Al_{14}O_{32}$[28,29]	Floating zone, followed by Ca reduction	pXRD	No	Metallic
$Ca_{11.3}Al_{14}O_{32.3}$[30]	Zone melting	Neutron powder diffraction	Yes	Semiconductor

Figure 4. Summary for Experimental Results on Stable OVCs in Ba-Nb-O and Ca-Al-O Systems Reported in the Literature

Characterization techniques are labeled as powder X-ray diffraction (pXRD), single crystal X-ray diffraction (SC-XRD), energy-dispersive X-ray spectroscopy (EDS), and transmission electron microscopy (TEM). If the structure does not have a clearly defined vacancy site, it is labeled as reconstructed. Room temperature (RT) properties stand for the metallic or semiconductor nature of the compound based on the reported temperature dependence of the electronic conductivity. The synthesis field highlights key conditions for experimental realization of the specific material.

hull") of such ternary structures. This entails searching for configuration versus composition that lies on the energy convex hull,[14] which defines the phases with energy lower than a linear combination of any competing phases at the corresponding compositions. We create candidate configurations by considering a base compound ($BaNbO_3$, $Ba_3Nb_5O_{15}$, $Ca_6Al_7O_{16}$, or $Ag_3Al_{22}O_{34}$), then create a replica of N such units of the base compound and add successively p metal vacancies, i.e., OVC = $N \times$ (base) + pV_m, searching via total energy minimization for stable and metastable configurations. We also include experimentally known reconstructed OVCs, the compounds that satisfy the OVC expression but do not have clearly defined vacancy sites (e.g., $Ba_3Nb_5O_{15}$, $BaNb_2O_6$, and $Ba_5Nb_4O_6$).

Available information on the experimental literature[15–30] is provided in Figure 4, and the theoretical results of this work are summarized in Figure 5. The key point to notice is that there is a sequence of stable OVC phases, each having a specific concentration of electrons per formula unit (*e*/f.u.) in the CB (including possibly zero). This is illustrated in Figures 6A and 7A showing the ground state diagrams for Ba-Nb-O and Ca-Al-O systems and chemical potential stability diagrams (Figures 2A

OVC generator	Resulting OVC	N_e (*e/f.u*)	ΔE_{CB} (eV)	E_g^{int} (eV)	Material type	Symmetry
Ba-Nb-O						
1:1:3 (Base)	$BaNbO_3$	1	1.11	2.26	I	1:1:3
27×(1:1:3)+V_{Ba}	$Ba_{26}Nb_{27}O_{81}$	25/27	1.04	2.22	I	1:1:3-like
10×(1:1:3)+V_{Ba}	$Ba_9Nb_{10}O_{30}$	8/10	0.90	2.19	I	1:1:3-like
8×(1:1:3)+V_{Ba}	$Ba_7Nb_8O_{24}$	6/8	0.88	2.17	I	1:1:3-like
7×(1:1:3)+V_{Nb}	**$Ba_7Nb_6O_{21}$**	**2/7**	**0.40**	**2.20**	**II**	**Reconstructed**
5×(1:1:3)+2V_{Ba}	**$Ba_3Nb_5O_{15}$**	**1/5**	**0.46**	**1.87**	**II**	**Reconstructed**
2×(1:1:3)+V_{Ba}	$BaNb_2O_6$	0	0	2.72	III	Reconstructed
5×(1:1:3)+V_{Nb}	$Ba_5Nb_4O_{15}$	0	0	2.65	III	Reconstructed
Ca-Al-O						
6:7:16 (Base)	$Ca_6Al_7O_{16}$	1	0.96	3.49	I	6:7:16
4×(6:7:16)+V_{Ca}	**$Ca_{23}Al_{28}O_{64}$**	**2/4**	**0.67**	**3.10**	**II**	**6:7:16-like**
2×(6:7:16)+V_{Ca}	$Ca_{11}Al_{14}O_{32}$	0	0	3.40	III	6:7:16-like

Figure 5. Summary of the Computational Results on Stable OVCs in Ba-Nb-O and Ca-Al-O Systems

The OVCs are generated by creating supercells of a base cell as OVC = N × (base) + pV_m, where N and p are integer numbers. Number of electrons (N_e) in the conduction band is given per formula unit (f.u.) of the base compound (i.e., $BaNbO_3$ or $Ca_6Al_7O_{16}$). In general, the number of electrons in the conduction band for the degenerate gapped Ca-Al-O and Ba-Nb-O compounds can be predicted from the sum of composition-weighted formal oxidation states assuming Ba^{2+}, Ca^{2+}, Al^{3+}, Nb^{5+}, and O^{2-} for each material. ΔE_{CB} is the occupied energy range of conduction band and E_g^{int} is the internal gap between CBM and VBM (Figure 1A) estimated from the density of states. Types of materials I, II, and III stand for non-transparent metals, potentially TCs (shown in red), and insulators, respectively. If the OVC in the lowest energy state does not have clearly defined vacancy sites, it is labeled as reconstructed.

and 7B) demonstrating the phases that are stabilized as the chemical potentials of the atoms being removed are continuously changed between their allowed values. Finally, we show how a window of opportunity can be determined computationally between opposing tendencies of (1) stability (Figures 2A and 7B), (2) conductivity (Figures 6B–6D and 7C), and (3) transparency (Figure 8) to design new TCs.

Stable Phases and OVCs for the Ba-Nb-O System

Computationally, we find 25 binary and ternary ground state compounds (described in Data S1) of which $Ba_7Nb_6O_{21}$, $Ba_5Nb_4O_{15}$, $Ba_3Nb_5O_{15}$, $Ba_7Nb_8O_{24}$, $Ba_9Nb_{10}O_{30}$, $Ba_{26}Nb_{27}O_{81}$, and $BaNb_2O_6$ are OVCs (Figure 5). Here, 7:8:24, 9:10:30, and 26:27:82 phases have clearly defined vacancy sites, and 1:2:6, 3:5:15, and 5:4:15 OVCs are reconstructed compounds observed experimentally before.[19,26,27,31,32] It should be noted that for the perovskite $BaNbO_3$ (Figure 4), there has been a focused effort to quantify the occupancy of the A site via diffraction, and authors have noted that there are possible vacancies, as "…slight departures of the stoichiometry below the detection limits of the neutron powder diffraction technique cannot be

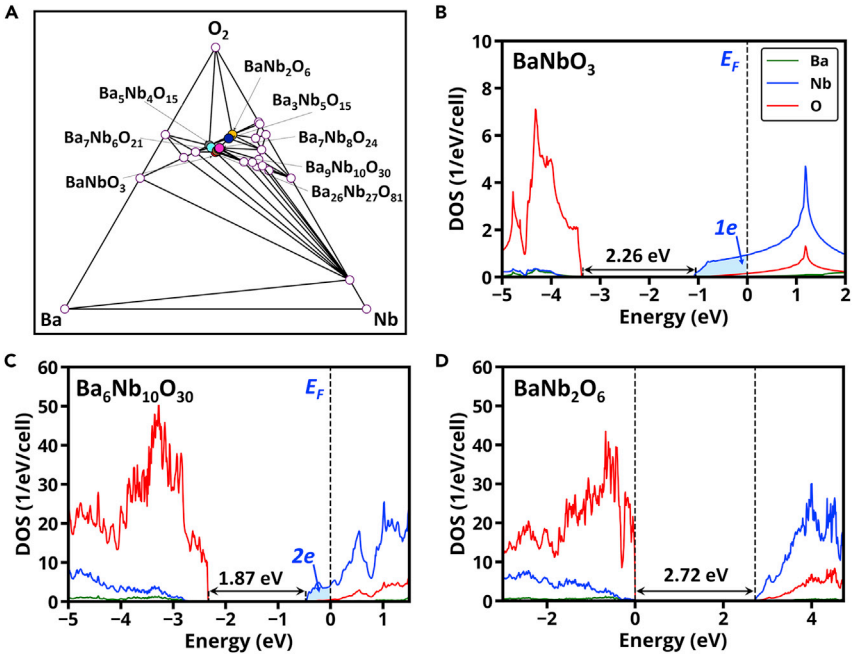

Figure 6. Stability and Electronic Structures of $BaNbO_3$ and Its OVCs

(A) Convex hull for the Ba-Nb-O system indicating the OVCs in color. In Figure 3B, the OVCs were not included in the calculations of the stability green zone of $BaNbO_3$, but they are included in (A) and Figure 2A. This redefines the chemical potential stability zone under which the base compound can exist, and consequently the formation energy of Ba vacancy in $BaNbO_3$ is about 0 eV under the redefined cation-poor conditions.

Density of states for (B) $BaNbO_3$, (C) $Ba_6Nb_{10}O_{30}$, and (D) $BaNb_2O_6$, indicating the number of electrons in the conduction band per formula unit.

excluded."[18] Indeed, several potential experimental compositions (i.e., $Ba_{0.95}NbO_3$ and $Ba_{0.97}NbO_3$) nearly match predicted phases ($Ba_{26}Nb_{27}O_{81} \approx Ba_{0.963}NbO_3$), whereas other predicted compositions (i.e., $Ba_7Nb_8O_{24}$ and $Ba_9Nb_{10}O_{30}$) exceed the observed vacancy concentration.

Stable Phases and OVCs for the Ca-Al-O System

We identify computationally a total of ten binary and ternary ground state compounds (described in Data S2) of which $Ca_{11}Al_{14}O_{32}$ and $Ca_{23}Al_{28}O_{64}$ are OVCs (Figure 5). Here, both OVCs have clearly defined vacancy sites with the long-range ordering of Ca vacancies. Despite the limited information on the formation of non-stoichiometric $Ca_{6-x}Al_7O_{16}$ systems (Figure 4), $Ca_{11.3}Al_{14}O_{32.3}$ compound with $Ca_6Al_7O_{16}$-like structure and partial occupancy of Ca sites has been reported experimentally,[30] which indirectly support our theoretical predictions.

Stable Phases and No OVCs for the Ag-Al-O System

We find computationally a total of four binary and ternary ground state compounds (described in Data S3): Al_2O_3, Ag_2O, AgAl, and $AgAlO_2$. None of them are OVCs. In fact, the $Ag_3Al_{22}O_{34}$ and its $Ag_2Al_{22}O_{34}$ OVC lie energetically above the convex hull by 0.034 and 0.01 eV/atom, respectively. Specifically, $Ag_3Al_{22}O_{34}$ decomposes to $AlAgO_2$, Ag, and Al_2O_3 phases, while $Ag_2Al_{22}O_{34}$ decomposes to $AgAlO_2$ and Al_2O_3. In other words, the formation of Ag vacancy is highly effective and drains all electrons from the CB; thus, $Ag_2Al_{22}O_{34}$ is an insulator. This vacancy formation increases the system stability (the energy above the convex hull is smaller for $Ag_2Al_{22}O_{34}$ than that for $Ag_3Al_{22}O_{34}$), but both $Ag_3Al_{22}O_{34}$ and $Ag_2Al_{22}O_{34}$ are

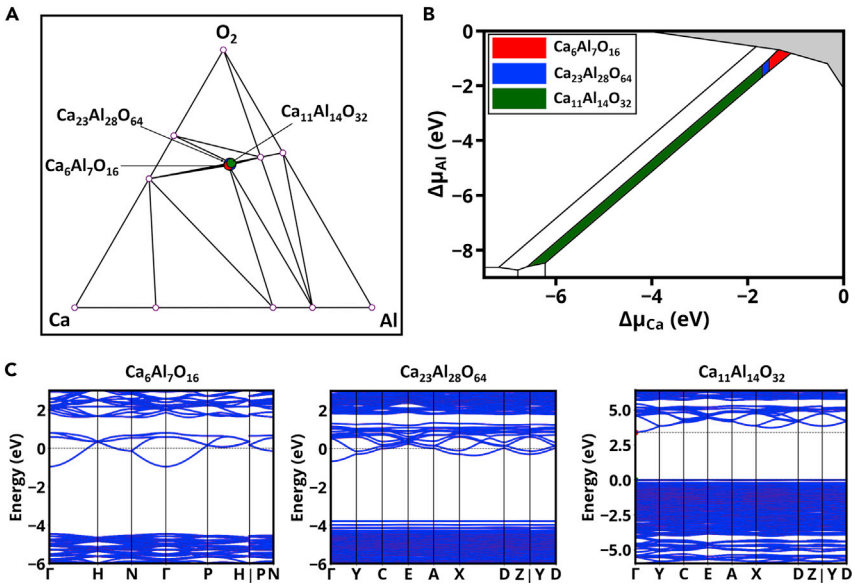

Figure 7. Stability and Electronic Structures of $Ca_6Al_7O_{16}$ and Its OVCs

(A) Convex hull for the Ca-Al-O system indicating the OVCs in color.

(B) Chemical potential diagram for the Ca-Al-O system, showing the stability chemical potential zone for each stable OVC phase in colors corresponding to the ground states in (A). The gray zone corresponds to the prohibitive chemical potential stability zone of binary Ca-Al systems. In Figure 3D, the OVCs were not included in the calculations of the stability green zone of $Ca_6Al_7O_{16}$, but they are included (A and B). This redefines the chemical potential stability zone under which the base compound can exist, and consequently the formation energy of Ca vacancy in $Ca_6Al_7O_{16}$ is about 0 eV under the redefined cation-poor conditions.

(C) Band structures for $Ca_6Al_7O_{16}$ and its OVCs.

unstable with respect to competing phases. Our experimental attempts to reduce synthesized $Ag_3Al_{22}O_{34.5}$ to $Ag_3Al_{22}O_{34}$ via heating the compound to 700°C to liberate oxygen results in the formation of free metallic silver and $Ag_{2.5}Al_{22}O_{34.25}$ (Note S1). These results suggest that despite the fact that $Ag_3Al_{22}O_{34}$ might be attractive as an intrinsic TC[5] if Ag vacancy formation can be partially inhibited, the system is not likely to be realized experimentally under normal conditions.

Different OVCs Have Different Number of Free Carriers, Absorption, and Conductivity

Trends in the Number of Electrons in the CB of Intrinsic TCs and the Metal-Insulator Transition

For the Ba-Nb-O system (Figure 5), among the ground state structures, the phases 1:1:3, 7:6:21, 26:27:81, 9:10:30, 7:8:24, and 3:5:15 have electrons in the CB and wide internal band gaps. From the sequences of OVCs, we find that both Ba and Nb vacancies act as acceptors, removing 2*e* and 5*e* per vacancy from the CB (Figures 6B–6D). The electronic properties of Ba-Nb-O systems were studied experimentally by various groups (Figure 4). Specifically, it has been shown that the 1:1:3 compound is a metal,[18] whereas the 1:2:6 and 5:4:15 OVCs are insulators.[26,27,33,34] At the same time, despite a few experimental works reporting low resistivity for the 3:5:15 compound, the temperature dependence of the resistivity (metal versus semiconductor nature) is different for different studies.[19–22,25] These results are not surprising considering the tiny range of chemical potentials under which the 3:5:15 OVC exists (Figure 2A), low defect formation energy in degenerate gapped compounds, and

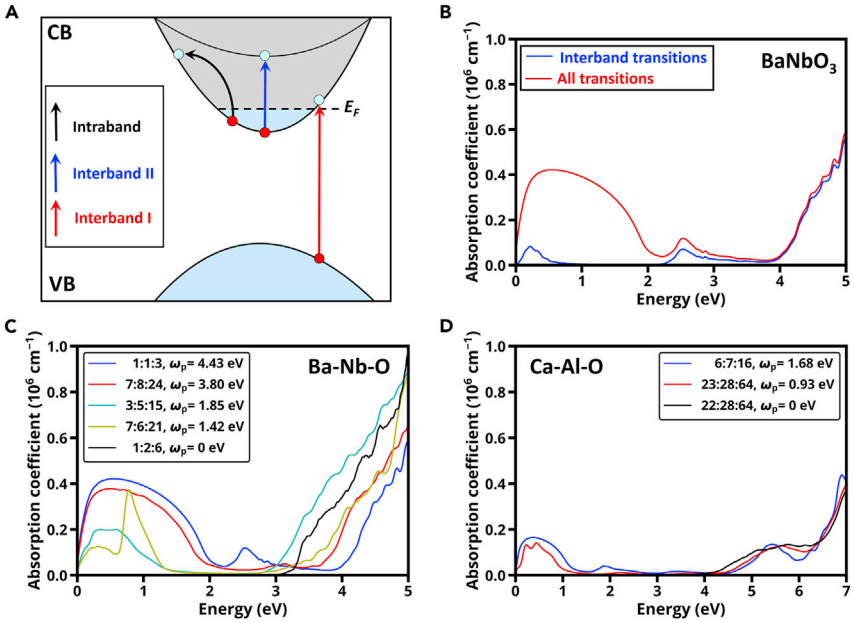

Figure 8. Effect of Non-stoichiometry on Optoelectronic Properties

(A) Schematic illustration of different contributions to optical properties in degenerate gapped compounds.

(B) Absorption spectra for $BaNbO_3$ considering only interband transitions and superposition of interband and intraband transitions.

(C) Effect of non-stoichiometry on the average absorption spectra of degenerate gapped compounds in the Ba-Nb-O system.

(D) Effect of non-stoichiometry on the average absorption spectra of degenerate gapped compounds in the Ca-Al-O system. The averaged plasma frequency over the three Cartesian directions is given for each system.

complexity of material synthesis. In our own work on 3:5:15 OVC, we see the preferential formation of the secondary reconstructed 1:2:6 and 5:4:15 OVCs over the targeted compound (Note S2). This reflects the narrow stability region of the 3:5:15 phase versus the reconstructed OVCs. Hence, the sensitivity of sample preparation conditions reignites the need for high-quality single crystals to quantify potential vacancy concentration and to understand the potential structural/electronic impact of vacancy formation.

For the Ca-Al-O system (Figure 5), from the analysis of electronic structures of the ground state compounds, we identify the phases 6:7:16 and 23:28:64 as degenerate gapped compounds with 1*e*/f.u. and 2*e*/f.u. in the CB, respectively. At the same time, the 11:14:32 OVC has no CB electrons, i.e., it is an insulator with a wide band gap. The results for electronic structures of OVCs suggest that Ca vacancy in 6:7:16-based degenerate gapped compounds acts as acceptor removing 2*e* from the CB. However, in contrast to the OVCs in the Ba-Nb-O system, the formation of Ca vacancy produces in-gap occupied defect states that reduce both the internal band gap energy and the energy range of occupied states (Figure 7C). The high electronic conductivity of 6:7:16 is known from experimental studies (Figure 4),[28,29] but the insulating and conducting properties of 11:14:32 and 23:28:64 OVCs are yet to be confirmed. It should also be noted that 6:7:24 and its 23:28:64 OVC have clearly defined 0-dimensional charge carrier density localization, which implies that both compounds are not only degenerate gapped compounds but also stable inorganic electrides (Note S3).

Spontaneously Formed Vacancies Enhance Transparency while Reducing Conductivity

The optical properties of a degenerate gapped compound are determined by superposition of interband and intraband transitions (Figure 8A). Owing to the occupied CB, the band-to-band transitions can be divided into (I) interband transitions from the occupied valence to unoccupied conduction bands and (II) interband transition from occupied conduction to higher energy unoccupied bands. In the simplified model used here, the intraband transitions can be predicted within the Drude model[35] describing free-electron absorption.

The contribution of the aforementioned different types of transitions to the absorption spectra is illustrated in Figure 8B for $BaNbO_3$. Specifically, the interband transitions (I) contribute to the absorption spectra at energies slightly above $E_g^{int} + \Delta E_{CB}$ due to the curvatures of the valence and conduction bands. The interband transitions (II) contribute noticeably at energies below those for interband transitions (I) and determine the absorption spectra in the range from 2 to 4 eV. Finally, the intraband contribution determines the low-energy region of absorption spectra. This analysis defines the design principles for good intrinsic TCs that require (1) metals with large internal gaps between the valence and conduction bands to minimize the interband absorption in visible range and (2) a high enough carrier density (n_e) in the CB to provide conductivity, while having (3) a low enough carrier density, limiting the interband transition in the CB and plasma frequency ($\omega_p \sim \sqrt{n_e/m}$, where m is an effective carrier mass), so that free-electron absorption does not impede the needed optical transparency. Furthermore, (4) the free carriers in the CB above the internal band gap should not destabilize the compound by spontaneously creating Fermi level-induced defects that defeat conductivity.

For the Ba-Nb-O system, the 1:1:3 degenerate gapped compound has the highest plasma frequency (ω_p = 4.43 eV) among the considered materials which results in strong Drude contribution in the visible light range. Hence, despite high carrier concentration ($n_e = 1.38 \times 10^{22}$ cm^{-3}) and stability, the 1:1:3 compound is not TC due to low transparency. Indeed, the 1:1:3 samples have clearly distinct color in experimental studies.[18] At the low vacancy concentration, the effect of the defects on carrier density and optical properties is negligible. However, the increase in Ba or Nb vacancy concentration and formation of OVCs noticeably change the optoelectronic properties via reducing plasma frequency contribution and modifying the material band structure. Although 26:27:81, 9:10:30, and 7:8:24 OVCs have smaller carrier concentrations compared with 1:1:3 compound, the free-electron absorption is still a limiting factor as shown in the example of 7:8:24 OVC (Figure 8C). Among the stable degenerate Ba-Nb-O gapped compounds, 3:5:15 and 7:6:21 compounds have the smallest average absorption coefficients in the visible range (highest transparency).

For the Ca-Al-O system, the optical properties of degenerate gapped materials in the visible range in large part are determined by the interband transition from occupied conduction to unoccupied bands. Specifically, for the 6:7:16 compound, the carrier concentration of 2.26×10^{21} cm^{-3} results in the averaged plasma frequency of 1.68 eV, which does not induce noticeable free-electron absorption in the visible range. The interband transitions from the valence to the conduction bands are well separated in energy and contribute only above $E_g^{int} + \Delta E_{CB}$, which is over 4.4 eV (Figure 7C). Because of this, the absorption in the visible light range is mainly determined by interband transitions in the CB finally resulting in colored material. The Ca vacancy formation removing 2*e* from the CB per defect not only reduces the plasma

frequency but also changes the interband transition, which is illustrated in the absorption spectra of 6:7:16 and its OVCs (see Figure 8D). In particular, 23:28:64 OVC has the lowest absorption in the visible light range among the considered degenerate gapped compounds.

Stability of OVCs during Growth Is the Knob that Controls Vacancy Concentration and Hence Transparency and Conductivity

We have seen above that different OVCs have a different number of free carriers, absorption, and conductivity. What makes this a useful feature is that each such OVC can be realized in a unique and specific range of atomic chemical potentials that can, in principle, be controlled during growth. This is illustrated in Figure 2A for the Ba-Nb-O system and in Figure 7B for the Ca-Al-O system, whereas $Ag_3Al_{22}O_{34}$ offers no control as the Ag vacancy forms readily for any chemical potential. Significantly, the results in Figures 2A and 7B suggest that it is possible to stabilize different $Ba_lNb_mO_n$ and $Ca_lAl_mO_n$ OVCs by tuning Ba/Nb and Ca chemical potentials, respectively. As an illustration, considering the chemical potential stability zone for $BaNbO_3$ (Figure 2A), we find that the reduction of the Ba chemical potential results in stabilization of the 26:27:81, 9:10:30, 7:8:24, 3:5:15, and 1:2:6 OVCs, while 7:6:21 and 5:4:15 OVCs are stable under Nb-poor conditions. Formation of non-stoichiometric structures for Ba-Nb-O materials family has also been reported experimentally (Figure 4); our results extend the knowledge on non-stoichiometric structures, showing how non-stoichiometry often seen in the system is an electronic effect—a high Fermi energy induces the formation of electron-killer cation vacancies. This effect is argued to be rather widespread, not an exotic curiosity, as there are many compounds with large internal gaps and Fermi level in the CB. For instance, fairly recently, $Sr_{1-x}NbO_3$ (a $BaNbO_3$-like metal whose Fermi level sits above a ~1.8 eV gap) was found to be rare, colored, metallic photocatalyst[11] whose coloring and electronic conductivity can be controlled by synthesis conditions. Our results also provide insights into the stability of the transparent conductive states while pointing out that controllable formation of non-stoichiometric degenerate gapped compounds can be used to design next-generation TCs. Specifically, among the stable OVCs, $Ba_3Nb_5O_{15}$, $Ba_7Nb_6O_{21}$, and $Ca_{23}Al_{28}O_{64}$ OVCs are potential TCs. However, $Ba_3Nb_5O_{15}$ exists only under an extremely tiny range of chemical potentials (see Figure 2A). Because of this and low defect formation energy in degenerate gapped compounds, the further research is required to quantify the sensitivity of sample preparation conditions on the structural/electronic properties of the material. $Ba_7Nb_6O_{21}$ and $Ca_{23}Al_{28}O_{64}$ OVCs are first predicted to be stable ground state compounds and constitute opportunities for novel synthesis. Here, $Ca_{23}Al_{28}O_{64}$ OVC has the highest transparency among all considered systems, but due to the small stability zone, a precise control of chemical potentials is needed to realize the compound. $Ba_7Nb_6O_{21}$ exists in the widest range of chemical potentials among the potential TCs, which implies a simpler control of synthesis conditions to realize the material.

Conclusions

The existence of non-stoichiometry in oxides is often thought to be a growth effect rather than a specific electronic instability. However, we demonstrate via first-principles calculations that a degenerate gapped compound with sufficiently large internal gap and Fermi level in the CB can have a characteristically negative cation vacancy formation enthalpy; in other words, spontaneous non-stoichiometry occurs even at low temperatures, intrinsic to the compound (not due to extrinsic effects). At the concentrated limit, such vacancies condense into OVCs. We show that this is a generic behavior as cation vacancy formation results in the decay of CB electrons into electron

acceptor states. As a result, the negative electron-hole recombination energy offsets the positive energy associated with vacancy bond breaking. Our results thus explain and clarify how non-stoichiometry often seen in oxides is an electronic effect—a high Fermi energy induces the formation of electron-killer acceptors. This effect is argued to be rather widespread, not an exotic curiosity, as there are many compounds with such electronic structures. We demonstrate by the chemical potential phase diagrams the growth regimes where a particular *l*:*m*:*n* OVC with a fixed level of transparency and conductivity is stable. For example, whereas in $Ag_3Al_{22}O_{34}$, the Ag vacancies form readily (so the CB is completely depleted of carriers), in the Ca-Al-O and Ba-Nb-O systems there are well-defined chemical potential domains, where OVCs with an optimal number of carriers persist. Since each *l*:*m*:*n* OVC depletes the CB of electrons by a different amount, the controllable formation of OVCs can be used to modify interband absorption, enhance materials stability, reduce plasma absorption, and design next-generation TCs. Specifically, we identify $Ba_3Nb_5O_{15}$, $Ba_7Nb_6O_{21}$, and $Ca_{23}Al_{28}O_{64}$ OVCs as attractive candidatures for TC application. This work has broad implications as degenerate gapped compounds have been attracting much interest in many fields beyond that of TCs.

EXPERIMENTAL PROCEDURES

Density Functional Calculations

All spin-polarized calculations were carried out using Perdew-Burke-Ernzerhof functional[36] with DFT+U correction for Nb (U = 1.5 eV) and Ag (U = 5 eV) d-like orbitals as implemented by Dudarev et al.[37] and available in Vienna Ab Initio Simulation Package.[38] Although the DFT+U approach is a simplified self-interaction correction, it appears to describe correctly both reduced ligand states ("trapped holes") as well as ligands with conventional formal oxidation states, as demonstrated in tests described in literature.[39,40] It should be noted that the utilization of DFT+U with a larger U value (i.e., U = 3 eV) for Nb d-like orbitals results in incorrect insulating nature of the $BaNbO_3$ system. The cutoff energies for plane-wave basis were set to 500 and 600 eV for the final static and volume relaxation calculations, respectively. Γ-centered Monkhorst-Pack k-grids[41] were used in the Brillouin-zone integrations with grid densities of approximately 2,500 and 10,000 per reciprocal atom for volume relaxation and final static calculations. For each system, random atomic displacements within 0.1 Å were applied to avoid trap at a local minimum. The full optimization of lattice vectors and atomic positions was allowed. The results were analyzed using VESTA[42] and pymatgen.[43]

Calculations of Chemical Potential Domains

To calculate stability zones for $BaNbO_3$, $Ca_6Al_7O_{16}$, and $Ag_3Al_{22}O_{34}$ compounds presented in Figure 3, we used only experimentally known stoichiometric crystal structures available in the Inorganic Crystal Structure Database (ICSD)[6] and SpringerMaterial.[44] To predict convex hulls and chemical potential diagrams for Ca-Al-O and Ag-Al-O systems, in addition to the known experimental structures, we included generated OVCs and structures available in the Materials Project[45] database. For the Ba-Nb-O system (Figures 2A and 6A), we also considered stoichiometries inspired by II-V-O phase diagrams. The O_2 molecule was used as a reference state for the O_2 phase. The ground state compounds found in this work are given in Data S1–S3. We implemented fitted elemental-phase reference energy corrections[46] to correct chemical potentials for elemental reference states.

Optical Spectra

The optical properties (Figure 8) were computed within independent particle approximation.[47] To calculate plasma frequencies and interband transition spectra,

40 × 40 × 40, 20 × 20 × 20, 20 × 20 × 20, 8 × 24 × 8, 16 × 12 × 8, 20 × 20 × 20, 8 × 8 × 8, and 8 × 8 × 8 Γ-centered k-point grids were used for $BaNbO_3$, $Ba_7Nb_8O_{24}$, $Ba_7Nb_6O_{21}$, $Ba_3Nb_5O_{15}$, $BaNb_2O_6$, $Ca_6Al_7O_{16}$, $Ca_{23}Al_{28}O_{64}$, and $Ca_{11}Al_{14}O_{32}$, respectively. The Drude contribution to optical properties was included by utilizing kram code[48] with plasma frequencies calculated from first-principles calculations and the damping coefficient of 0.2 eV, which is analogous to traditional TCs.[49]

Defect Calculations

Supercells with 116, 135, and 236 atoms were used to calculate defect energetics in $Ca_6Al_7O_{16}$, $BaNbO_3$, and $Ag_3Al_{22}O_{34}$ systems, respectively. The defect formation energies (Figures 3A, 3C, and 3E) and finite size corrections were computed within the framework described by Lany and Zunger[50,51] and implemented in the pyladadefects code.[52] For the defect calculations, the ranges of chemical potentials were determined using only experimentally known stoichiometric crystal structures as described above. It should be noted that unlike conventional insulators where the Fermi energy can span the full range of the gap (Figure 1B), thus controlling the balance between different charges, if the Fermi energy resides inside a continuum band, as is the case in Figure 1A, it represents the energy to add or remove an electron from the host system, not from point defects in the gap. Thus, the conventional calculation of charged defects versus E_F is not meaningful in degenerate gapped materials.

DATA AND SOFTWARE AVAILABILITY

All data needed to evaluate the conclusions in the paper are present in the paper and the Supplemental Information. Additional data related to this paper may be requested from the authors.

SUPPLEMENTAL INFORMATION

Supplemental Information can be found online at https://doi.org/10.1016/j.matt.2019.05.014.

ACKNOWLEDGMENTS

The work of A.Z. and O.I.M. at University of Colorado Boulder, and of K.R.P. and M.T.Y. at Northwestern University, was supported by the NSF-DMR EPM program under grants DMR-1806939 and DMR-1806912, respectively. M.T.Y. would like to thank the Department of Energy (DOE) Office of Energy Efficiency and Renewable Energy (EERE) Postdoctoral Research Award under the EERE Solar Energy Technologies Office administered by the Oak Ridge Institute for Science and Education (ORISE) for the DOE. The ORISE is managed by Oak Ridge Associated Universities (ORAU) under DOE contract number DE-SC00014664. All opinions expressed in this paper are the authors' and do not necessarily reflect the policies and views of DOE, ORAU, or ORISE. O.I.M. and C.P. acknowledge support from the Research Council of Norway (contract no. 251131), and the Norwegian Metacenter for Computational Science (NOTUR) for providing access to supercomputer resources. We would like to thank Zachary Mansley for help with transmission electron microscopy.

AUTHOR CONTRIBUTIONS

O.I.M. carried out the theoretical calculations. M.T.Y. fabricated the samples and carried out structure analysis by X-ray powder diffraction. A.Z. directed the design of the research, analysis of the results, and writing of the paper. O.I.M. contributed most to writing of the paper, with contributions from all co-authors. K.R.P. supervised the experimental work. C.P. and A.Z. supervised all theoretical studies.

DECLARATION OF INTERESTS

The authors declare no competing interests.

Received: January 1, 2019
Revised: April 9, 2019
Accepted: May 13, 2019
Published: July 10, 2019

REFERENCES

1. Dalton, J. (1808). A New System of Chemical Philosophy, *Vol. 1* (W. Dawson).
2. Berthollet, C.-L. (1803). Essai de statique chimique, *Vol. 2* (F. Didot).
3. D.S. Ginley, H. Hosono, and D.C. Paine, eds. (2010). Handbook of Transparent Conductors (Springer Science & Business Media).
4. Zhang, S.B., Wei, S.H., and Zunger, A. (1999). Overcoming doping bottlenecks in semiconductors and wide-gap materials. Phys. B Condens. Matter *273-274*, 976–980.
5. Zhang, X., Zhang, L., Perkins, J.D., and Zunger, A. (2015). Intrinsic transparent conductors without doping. Phys. Rev. Lett. *115*, 176602.
6. Belsky, A., Hellenbrandt, M., Karen, V.L., and Luksch, P. (2002). New developments in the inorganic crystal structure database (ICSD): accessibility in support of materials research and design. Acta Crystallogr. B *58*, 364–369.
7. Hart, G.L.W., and Zunger, A. (2001). Origins of nonstoichiometry and vacancy ordering in $Sc_{1-x}\square_xS$. Phys. Rev. Lett. *87*, 275508.
8. Zhang, S.B., Wei, S.-H., and Zunger, A. (1997). Stabilization of ternary compounds via ordered arrays of defect pairs. Phys. Rev. Lett. *78*, 4059–4062.
9. Anand, S., Xia, K., Zhu, T., Wolverton, C., and Snyder, G.J. (2018). Temperature dependent n-type self doping in nominally 19-electron half-Heusler thermoelectric materials. Adv. Energy Mater. *8*, 1801409.
10. Anand, S., Xia, K., Hegde, V.I., Aydemir, U., Kocevski, V., Zhu, T., Wolverton, C., and Snyder, G.J. (2018). A valence balanced rule for discovery of 18-electron half-Heuslers with defects. Energy Environ. Sci. *11*, 1480–1488.
11. Xu, X., Randorn, C., Efstathiou, P., and Irvine, J.T.S. (2012). A red metallic oxide photocatalyst. Nat. Mater. *11*, 595–598.
12. Kitano, M., Inoue, Y., Yamazaki, Y., Inoue, Y., Yamazaki, Y., Hayashi, F., Kanbara, S., Matsuishi, S., Yokoyama, T., Kim, S.W., Hara, M., Hosono, H., et al. (2012). Ammonia synthesis using a stable electride as an electron donor and reversible hydrogen store. Nat. Chem. *4*, 934–940.
13. Hosono, H., Kim, J., Toda, Y., Kamiya, T., and Watanabe, S. (2017). Transparent amorphous oxide semiconductors for organic electronics: application to inverted OLEDs. Proc. Natl. Acad. Sci. USA *114*, 233–238.
14. Ducastelle, F. (1991). Order and Phase Stability in Alloys (North-Holland).
15. Svensson, G. (1988). $Ba_2Nb_5O_9$ — an intergrowth of $BaNbO_3$ (perovskite) and NbO. Mater. Res. Bull. *23*, 437–446.
16. Svensson, G., and Werner, P.-E. (1990). Determination of the composition of $BaNbO_3$ using profile refinement and phase analysis. Mater. Res. Bull. *25*, 9–14.
17. Hessen, B., Sunshine, S.A., Siegrist, T., and Jimenez, R. (1991). Crystallization of reduced strontium and barium niobate perovskites from borate fluxes. Mater. Res. Bull. *26*, 85–90.
18. Casais, M.T., Alonso, J.A., Rasines, I., and Hidalgo, M.A. (1995). Preparation, neutron structural study and characterization of $BaNbO_3$ - a Pauli-like metallic perovskite. Mater. Res. Bull. *30*, 201–208.
19. Hessen, B., Sunshine, S.A., Siegrist, T., Fiory, A.T., and Waszczak, J.V. (1991). Structure and properties of reduced barium niobium oxide single-crystals obtained from borate fluxes. Chem. Mater. *3*, 528–534.
20. Hwang, Y.K., and Kwon, Y.-U. (1997). Syntheses and electrical properties of tetragonal tungsten bronze type solid solution $Ba_{6-x}La_xNb_{10}O_{30+\delta}$ (x = 0, 1, 2, 3) and $Sr_6Nb_{10}O_{30}$. Mater. Res. Bull. *32*, 1495–1502.
21. D'yachenko, O.G., Istomin, S.Y., Fedotov, M.M., Antipov, E.V., Svensson, G., Nygren, M., and Holm, W. (1997). Structure and properties of $Ba_{6-x}Ln_xNb_{10}O_{30}$, Ln = La, Ce and Nd compounds. Mater. Res. Bull. *32*, 409–419.
22. Kolodiazhnyi, T., Sakurai, H., Isobe, M., Matsushita, Y., Forbes, S., Mozharivskyj, Y., Munsie, T.J.S., Luke, G.M., Gurak, M., and Clarke, D.R. (2015). Superconductivity and crystal structural origins of the metal-insulator transition in $Ba_{6-x}Sr_xNb_{10}O_{30}$ tetragonal tungsten bronzes. Phys. Rev. B *92*, 214508.
23. Kolodiazhnyi, T., Sakurai, H., Vasylkiv, O., Borodianska, H., and Mozharivskyj, Y. (2014). Abnormal thermal conductivity in tetragonal tungsten bronze $Ba_{6-x}Sr_xNb_{10}O_{30}$. Appl. Phys. Lett. *104*, 111903.
24. Chan, J.H., Bock, J.A., Guo, H., Trolier-McKinstry, S., and Randall, C.A. (2017). Filled oxygen-deficient strontium barium niobates. J. Am. Ceram. Soc. *100*, 774–782.
25. Chan, J.H., Bock, J.A., Guo, H., Trolier-McKinstry, S., and Randall, C.A. (2017). High-temperature thermoelectric characterization of filled strontium barium niobates: power factors and carrier concentrations. J. Mater. Res. *32*, 1160–1167.
26. Galasso, F., Layden, G., and Ganung, G. (1968). ANb_2O_6 and ATa_2O_6 phases. Mater. Res. Bull. *3*, 397–407.
27. Galasso, F., and Katz, L. (1961). Preparation and structure of $Ba_5Ta_4O_{15}$ and related compounds. Acta Cryst. *14*, 647–650.
28. Matsuishi, S., Toda, Y., Miyakawa, M., Hayashi, K., Kamiya, T., Hirano, M., Tanaka, I., and Hosono, H. (2003). High-density electron anions in a nanoporous single crystal: $[Ca_{24}Al_{28}O_{64}]^{4+}(4e^-)$. Science *301*, 626–629.
29. Miyakawa, M., Kim, S.W., Hirano, M., Kohama, Y., Kawaji, H., Atake, T., Ikegami, H., Kono, K., and Hosono, H. (2007). Superconductivity in an inorganic electride 12CaO center dot $7Al_2O_3{:}e^-$. J. Am. Chem. Soc. *129*, 7270–7271.
30. Christensen, A.N. (1987). Neutron powder diffraction profile refinement studies on $Ca_{11.3}Al_{14}O_{32.3}$ and $CaCiO(D_{0.88}H_{0.12})$. Acta Chem. Scand. A *41*, 110–112.
31. Sirotinkin, S., Sirotinkin, V., and Trunov, V. (1990). Structure of low-temperature modification of $BaNb_2O_6$. Zh. Neorgan. Khim. *35*, 1609–1611.
32. Vanderah, T.A., Collins, T.R., Wong-Ng, W., Roth, R.S., and Farber, L. (2002). Phase equilibria and crystal chemistry in the BaO–Al_2O_3–Nb_2O_5 and BaO–Nb_2O_5 systems. J. Alloys Compd. *346*, 116–128.
33. Cho, I.-S., Bae, S.T., Kim, D.H., and Hong, K.S. (2010). Effects of crystal and electronic structures of ANb_2O_6 (A=Ca, Sr, Ba) metaniobate compounds on their photocatalytic H_2 evolution from pure water. Int. J. Hydrogen Energy *35*, 12954–12960.
34. Miseki, Y., Kato, H., and Kudo, A. (2006). Water splitting into H_2 and O_2 over $Ba_5Nb_4O_{15}$ photocatalysts with layered perovskite structure prepared by polymerizable complex method. Chem. Lett. *35*, 1052–1053.
35. Drude, P. (1900). Zur elektronentheorie der Metalle. Ann. Phys. (Berl.) *306*, 566–613.
36. Perdew, J.P., Burke, K., and Ernzerhof, M. (1996). Generalized gradient approximation made simple. Phys. Rev. Lett. *77*, 3865–3868.
37. Dudarev, S.L., Botton, G.A., Savrasov, S.Y., Humphreys, C.J., and Sutton, A.P. (1998). Electron-energy-loss spectra and the structural stability of nickel oxide: an LSDA+U study. Phys. Rev. B *57*, 1505–1509.
38. Kresse, G., and Furthmüller, J. (1996). Efficiency of ab-initio total energy calculations for metals and semiconductors using a plane-wave basis set. Comp. Mater. Sci. *6*, 15–50.

39. Dalpian, G.M., Liu, Q., Varignon, J., Bibes, M., and Zunger, A. (2018). Bond disproportionation, charge self-regulation, and ligand holes in ABX_3 perovskites by density functional theory. Phys. Rev. B *98*, 075135.

40. Liu, Q., Dalpian, G.M., and Zunger, A. (2019). Antidoping in insulators and semiconductors having intermediate bands with trapped carriers. Phys. Rev. Lett. *122*, 106403.

41. Monkhorst, H.J., and Pack, J.D. (1976). Special points for Brillouin-zone integrations. Phys. Rev. B *13*, 5188–5192.

42. Momma, K., and Izumi, F. (2011). VESTA 3 for three-dimensional visualization of crystal, volumetric and morphology data. J. Appl. Crystallogr. *44*, 1272–1276.

43. Ong, S.P., Richards, W.D., Jain, A., Hautier, G., Kocher, M., Cholia, S., Gunter, D., Chevrier, V.L., Persson, K.A., and Ceder, G. (2013). Python Materials Genomics (pymatgen): a robust, open-source python library for materials analysis. Comp. Mater. Sci. *68*, 314–319.

44. SpringerMaterials, The Landolt–Börnstein Database. https://materials.springer.com/.

45. Jain, A., Ong, S.P., Hautier, G., Chen, W., Richards, W.D., Dacek, S., Cholia, S., Gunter, D., Skinner, D., Ceder, G., and Persson, K.A. (2013). Commentary: the Materials Project: a materials genome approach to accelerating materials innovation. APL Mat. *1*, 011002.

46. Stevanović, V., Lany, S., Zhang, X., and Zunger, A. (2012). Correcting density functional theory for accurate predictions of compound enthalpies of formation: fitted elemental-phase reference energies. Phys. Rev. B *85*, 115104.

47. Gajdoš, M., Hummer, K., Kresse, G., Furthmüller, J., and Bechstedt, F. (2006). Linear optical properties in the projector-augmented wave methodology. Phys. Rev. B *73*, 045112.

48. Blaha, P., Schwarz, K., Madsen, G.K.H., Kvasnicka, D., Luitz, J., Laskowski, R., Tran, F., and Marks, L.D. (2001). WIEN2k, an Augmented Plane Wave + Local Orbitals Program for Calculating Crystal Properties (Karlheinz Schwarz, Technische Universität Wien).

49. Naik, G.V., Kim, J., and Boltasseva, A. (2011). Oxides and nitrides as alternative plasmonic materials in the optical range [Invited]. Opt. Mater. Express *1*, 1090–1099.

50. Lany, S., and Zunger, A. (2008). Assessment of correction methods for the band-gap problem and for finite-size effects in supercell defect calculations: case studies for ZnO and GaAs. Phys. Rev. B *78*, 235104.

51. Lany, S., and Zunger, A. (2009). Accurate prediction of defect properties in density functional supercell calculations. Modell. Simul. Mater. Sci. Eng. *17*, 084002.

52. Goyal, A., Gorai, P., Peng, H., Lany, S., and Stevanović, V. (2017). A computational framework for automation of point defect calculations. Comp. Mater. Sci. *130*, 1–9.